Assessment of 2D and 3D fractal dimension measurements of trabecular bone from high-spatial resolution magnetic resonance images at 3 T

Angel Alberich-Bayarri[a)]
Department of Radiology, Hospital Quirón Valencia, Valencia 46010, Spain

Luis Marti-Bonmati
Department of Radiology, Hospital Quirón Valencia, Valencia 46010, Spain and Department of Radiology, Hospital Universitario Dr. Peset, Valencia 46017, Spain

Maria Angeles Pérez
Group of Structural Mechanics and Materials Modeling, Aragon Institute of Engineering Research (I3A), University of Zaragoza, Zaragoza 50018, Spain

Roberto Sanz-Requena
Department of Radiology, Hospital Quirón Valencia, Valencia 46010, Spain

Juan José Lerma-Garrido
Department of Rheumatology, Hospital Quirón Valencia, Valencia 46010, Spain

Gracián García-Martí
Department of Radiology, Hospital Quirón Valencia, Valencia 46010, Spain and CIBER Mental Health Network, ISCIII, Valencia 46010, Spain

David Moratal
Center for Biomaterials and Tissue Engineering, Universidad Politécnica de Valencia, Valencia 46022, Spain

(Received 23 November 2009; revised 31 May 2010; accepted for publication 9 July 2010; published 26 August 2010)

Purpose: *In vivo* two-dimensional (2D) fractal dimension (D^{2D}) analysis of the cancellous bone at 1.5 T has been related to bone structural complexity and shown to be a potential imaging-based biomarker for osteoporosis. The objectives of this study were to assess at 3 T the *in vivo* feasibility of three-dimensional (3D) bone fractal dimension (D^{3D}) analysis, analyze the relationship of D^{2D} and D^{3D} with osteoporosis, and investigate the relationship of D^{3D} with spinal bone mineral density (BMD).

Methods: A total of 24 female subjects (67 ± 7 yr old, mean $\pm$ SD) was included in this study. The cohort consisted of 12 healthy volunteers and 12 patients with osteoporosis. MR image acquisitions were performed in the nondominant metaphysis of the distal radius with a 3 T MR scanner and an isotropic resolution of 180 μm. After segmentation and structural reconstruction, 2D and 3D box-counting algorithms were applied to calculate the fractal complexity of the cancellous bone. D^{2D} and D^{3D} values were compared between patients with osteoporosis and healthy subjects, and their relationship with radius BV/TV and spinal BMD was also assessed.

Results: Significant differences between healthy subjects and patients with osteoporosis were obtained for D^{3D} ($p<0.001$), with less differentiation for D^{2D} ($p=0.04$). The relationship between fractal dimension and BMD was not significant ($r=0.43$, $p=0.16$ and $r=0.23$, $p=0.48$, for D^{2D} and D^{3D}, respectively).

Conclusions: The feasibility of trabecular bone D^{3D} calculations at 3 T and the relationship of both D^{2D} and D^{3D} parameters with osteoporosis were demonstrated, with a better differentiation for the 3D method. Furthermore, the D^{3D} parameter has probably a different nature of information regarding the trabecular bone status not directly explained by BMD alone. Future studies with subjects with osteopenia and larger sample sizes are warranted to further establish the potential of D^{2D} and D^{3D} in the study of osteoporosis. © *2010 American Association of Physicists in Medicine*.
[DOI: 10.1118/1.3481509]

Key words: trabecular bone, magnetic resonance imaging, fractal dimension, image processing, osteoporosis

I. INTRODUCTION

Osteoporosis is a bone disorder that supposes a global concern affecting nearly 200 million people worldwide.[1] This syndrome is characterized by a decreased density of the bone tissue and deterioration in the trabecular bone architecture, both factors inducing an increased bone fragility and higher fracture risk. Osteoporosis is prevalent in women, especially in postmenopausal ages, leading to pain and disability associated with bone fractures.[2]

The diagnosis and monitoring of the disease is currently performed in the clinical setting by the quantification of the bone mineral density (BMD) by means of dual energy x-ray absorptiometry (DXA) technique. However, it has been demonstrated that not only the quantity of bone loss is important but also the heterogeneous nature of the trabeculae atrophy.[3] Advances on computed tomography (CT), high-resolution peripheral quantitative computed tomography (HR-pQCT), and magnetic resonance imaging (MRI) have allowed the research of *in vivo* characterization of cancellous bone microarchitecture.[4–6] The high inherent contrast between bone and bone marrow besides its nonionizing radiations place high field MRI as an especially suited technique for the *in vivo* structural characterization of trabecular bone.

Quantification of the trabecular bone has been mainly based on the calculation of morphometry measurements like apparent trabecular thickness (Tb.Th), apparent trabecular separation (Tb.Sp), apparent trabecular number (Tb.N), and apparent bone volume to total volume ratio (BV/TV), which have been shown to be a valuable tool in the study of the trabecular network.[7–9] Other developed methods to virtually quantify topology, anisotropy, complexity, and mechanical response of the cancellous bone have also been investigated.[10–14]

Trabecular shape and surfaces complexity appear to be altered under pathological conditions, with less irregular and less complex bone surfaces.[15] Using the fractal theory, it is possible to quantify structures with complex form through the fractal dimension, a parameter that indicates how an irregular structure tends to fill space after the observation at different scales.[16] Although there are a large number of definitions of the fractal dimension concept with different computation methods, the box-counting dimension, which is also known as Minkowski–Bouligand dimension, Kolmogorov capacity, or Kolmogorov dimension, has been widely extended in medical image processing due to the easiness of implementation.[17]

Trabecular bone fractal dimension relationship with other bone quality parameters has been assessed in different studies by the application of the two-dimensional (2D) box-counting algorithm to images acquired with different modalities.[15,18,19] However, only a reduced number of studies have analyzed the three-dimensional (3D) complexity of the trabecular bone network by a generalization of the box-counting algorithm to volumetric reconstructions obtained from multidetector row CT (MDCT) and synchrotron microtomography images.[4,20] In MRI, the use of 3D algorithms for the quantification of trabecular bone properties has been limited at 1.5 T by the reduced achievable spatial resolution. However, at higher field strengths (e.g., 3 T), it is possible to improve the *in vivo* 3D characterization of the trabecular structure since isotropic voxels with higher spatial resolutions can be obtained without compromising the signal-to-noise ratio (SNR).[6]

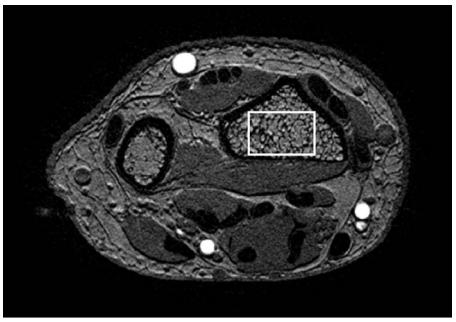

(a)

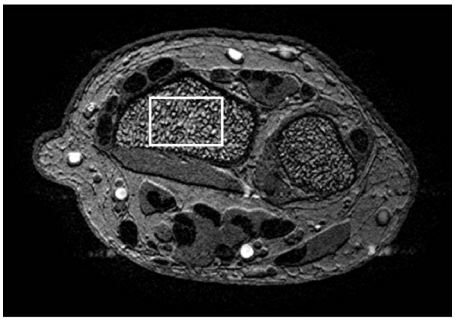

(b)

FIG. 1. Example of two acquired axial images with the 3D spoiled T1-weighted gradient echo sequence and corresponding selection of the ROI in one slice. Wrist slice corresponding to the acquisition performed in a left-handed 64 yr old female patient with osteoporosis (a). Image corresponding to a series acquired in a right-handed 62 years old female healthy volunteer (b).

The objectives of this study were to assess at 3 T the *in vivo* feasibility of 3D bone fractal dimension (D^{3D}) analysis, analyze the relationship of D^{2D} and D^{3D} with osteoporosis, and investigate the relationship of D^{2D} and D^{3D} with radius BV/TV and spinal BMD.

II. MATERIALS AND METHODS

II.A. Subjects

A total of 24 female subjects, with an age ranging from 54 to 80 yr old (67 ± 7 yr, mean $\pm$ SD), was included in the study after signing the corresponding informed consent. The study group comprises a cohort of 12 healthy subjects without history of bone diseases or bone fractures and a set of 12 patients meeting World Health Organization (WHO) criteria for the diagnosis of osteoporosis and reported bone fractures in the past 5 years, which were included in the group of patients with osteoporosis. Both healthy and osteoporotic populations were comparable regarding age (64 ± 7 yr vs 69 ± 7 yr, healthy vs osteoporotic; $p=0.06$, Student's t-test).

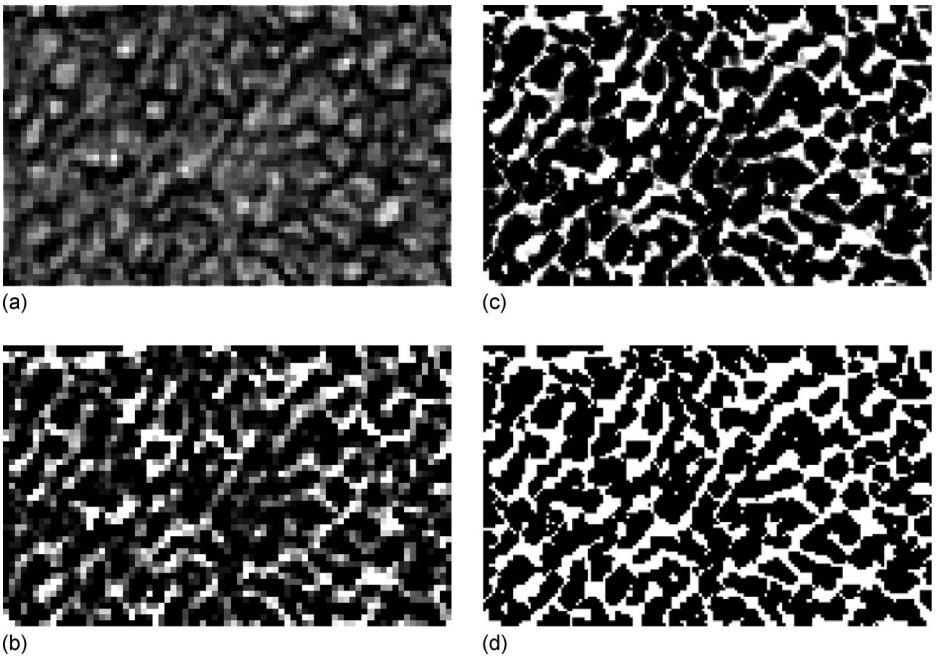

FIG. 2. Representative images resulting from the application of the different implemented preprocessing algorithms, region corresponds to the ROI selected in Fig. 1(b). Example of the isolated region exclusively containing trabecular bone and marrow (a). Image resulting from the application of the coil shading correction through the local intensity determination (b). Interpolated image after the execution of the subvoxel processing algorithm for an apparently increased spatial resolution (c). Binarized image obtained at the end of the preprocessing chain where only complete bone or marrow voxels exist (d).

II.B. Magnetic resonance imaging

The metaphysis of the nondominant distal radius was imaged using a 3 T magnetic resonance (MR) scanner (Achieva, Philips Healthcare, Best, The Netherlands). The gradient system consisted of a Dual Quasar, with a slew rate of 200 $\mathrm{mT/m\,ms^{-1}}$ and a maximal gradient strength of 80 mT/m. A four-channel phased-array surface coil especially designed for the wrist region was used for signal reception.

Images were obtained with a 3D spoiled T1-weighted gradient echo sequence (TE=5 ms, TR=16 ms, and FA=25°). The acquisition matrix size was of 512×512 pixels with 60 axial partitions. The slice thickness and pixel size were set to achieve isotropic voxels of 180 μm per edge. In order to improve SNR and contrast between bone and marrow, the number of acquisitions was set to 3, with a water-fat shift of 2.6 pixels (receiver bandwidth of 167.6 Hz/pixel). Parallel imaging techniques were used in the in-plane phase direction with an acceleration factor of 2 since they have been shown to be feasible in high-spatial resolution MRI acquisitions of the trabecular bone.[21] The total acquisition time was 5 min and 42 s.

II.C. Bone mineral density

Areal BMD of lumbar spine was also obtained only for the osteoporotic patients at the L2-L3-L4 vertebrae using a DXA scanner (Norland XR-46, Norland Corp, Fort Atkinson, USA). The BMD analysis was not performed in the healthy control subjects since it was not indicated in the clinical workflow. Subjects did not present any bone disease or related symptoms, and therefore they skipped the step of BMD evaluation with the DXA technique. Measures of BMD were given in $\mathrm{g/cm^2}$.

II.D. Image processing

MR image processing and analysis were performed in a workstation (Quad Core at 2.83 GHz and 8 GB of RAM memory) using MATLAB R2007a (The MathWorks, Inc., Natick, MA). Processing was automatic, and human interaction was only required at the initial segmentation step. Data processing and analysis was around 10 min per subject.

Segmentation of the trabecular bone from MR images was performed by placing a rectangular region of interest (ROI) in the first slice corresponding to the most proximal position and thereafter propagated to the rest of slices. Segmented areas were verified to exclusively contain marrow and trabecular bone (Fig. 1).

Slight modulations of the signal intensities across the acquisition volume, also known as coil shading phenomena, were corrected with nearest-neighbor statistics by the application of an implemented 3D local thresholding algorithm, as a generalization from its 2D version.[22] Marrow intensity values in the neighborhood of each voxel were determined and bone voxel intensities were scaled using calculated local intensities. Concretely, the method is based on the calculation of the average Laplacian values $\langle\tilde{L}\rangle_{\vec{r}}(I)$ in a sphere region $S(\vec{r})$ with a radius $R=15$ pixels, with I being the voxel intensity and $\vec{r}$ the center of the sphere, which is displaced through all voxels of the volume. When the calculated Laplacian equals zero $\langle\tilde{L}\rangle_{\vec{r}}(I_t(\vec{r}))=0$, the corresponding marrow intensity $I_t(\vec{r})$ can be determined locally. After the marrow intensity is obtained, it is used as a threshold and voxels can be directly classified into pure marrow voxels or scaled by its local threshold value and labeled as partially occupied by bone voxels (Fig. 2).[22]

The extreme conditions in terms of low SNR and partial volume effects due to larger voxel size than typical thickness

of the trabeculae, which is about 100–150 μm, forced the implementation of a method to increase the reconstructed spatial resolution. A subvoxel-processing algorithm was implemented to minimize partial volume effects and to improve the cancellous bone structural quantification from MRI.[23] The method consisted of a two-pass algorithm where each voxel was initially divided into eight subvoxels, which are assigned a level of intensity conditioned by the corresponding level of their voxel and near subvoxels, and also under the assumption that the amount of bone intensities must be conserved. In the first pass of the algorithm, each subvoxel was assigned an intensity value, depending on the intensities of the adjacent voxels and the local sum of intensities. The second pass of the algorithm consisted of the refinement of the previously calculated subvoxel intensities considering the intensities of the neighboring subvoxels and the total amount of intensity conservation.[23] Finally, an increased apparent isotropic spatial resolution of 90 μm was achieved and partial volume effects were minimized (Fig. 2).

The resulting images were binarized into exclusively bone or marrow voxels (Fig. 2). Histogram shape-based thresholding was implemented through the Otsu's method implemented in 3D. The method consists of the minimization of the intraclass variance of volume intensities,[24] which has been shown to be equivalent to maximizing the between-class variance. Thus, the optimum separation threshold was calculated for the entire volume using

$$t^* = \arg\max_t \frac{\sigma^2_B}{\sigma^2_T}, \tag{1}$$

where σ^2_T is the total variance and σ^2_B is the between-class variance. The optimum binarization threshold is t^*. Finally, voxels were classified as bone or marrow, depending on their intensity value. The corresponding BV/TV parameter of the processed volumes was directly calculated from this step since it was straightforward.

II.E. Fractal analysis

In order to calculate the trabecular bone D^{2D}, the conventional box-counting algorithm was implemented. A slice-by-slice contour detection routine implemented in MATLAB was included at the beginning of the code. For each slice, grids of different sizes were sequentially overlaid to the contour image. The total amount of grid boxes containing boundary pixels was calculated for each box size and stored in a vector. Box sizes were powers of 2 and the maximum box size was the smallest power of 2 above the largest dimension of the contour image. Once the number of boxes containing contour was obtained for each grid size, data were fitted by least mean squares according to

$$\log(N) = -D\log(\lambda) + \log(\alpha). \tag{2}$$

Equation (1) gives the relationship between the number of contour boxes (N), the corresponding box size (λ), the box-counting fractal dimension parameter (D), and a proportionality constant (α). Geometrically, D corresponds to the negative value of the slope of the line relating the natural logarithms of the number of boxes containing contour and each corresponding box sizes. The fractal dimension was calculated for each slice and the results were averaged in order to calculate the D^{2D} parameter of each scan. The 2D box-counting algorithm implemented for the quantification of 2D fractal complexity was validated by its application to the Sierpinski triangle figure, which has a known fractal dimension of $\log(3)/\log(2)=1.585$.

FIG. 3. 3D reconstruction of the trabecular bone with surface extraction after the application of the marching cubes algorithm. Inner volume and extracted trabeculae surfaces can be appreciated.

A generalized version of the box-counting algorithm was also developed and implemented for the quantification of the 3D trabecular bone complexity. The box-counting algorithm previously used for 2D calculations was herein extrapolated to the 3D space domain. Trabeculae surfaces were computed by the marching-cube algorithm before the application of the 3D box-counting method (Fig. 3). Different 3D cube meshes with varying cube sizes were generated and mixed with the 3D reconstruction of the trabecular bone surfaces. Analogously, the number of cubes containing trabecular surface was calculated for each cube size and stored in a vector. Cube size dimensions were generated similar to the 2D method and the maximum cube size was the smallest power of 2 over the largest dimension of the 3D surface matrix. The D^{3D} parameter was directly calculated by least mean squares fitting of the data to Eq. (1). The 3D box-counting method implemented was also validated by its application to the Menger sponge structure, which is characterized by a theoretic fractal dimension of $\log(20)/\log(3)=2.727$.

II.F. Statistical analysis

The statistical analysis was performed in SPSS 13.0 for Windows (SPSS, Inc., Chicago, IL). The ages and 2D and 3D fractal dimension parameters had a normal distribution (Kolmogorov–Smirnov test, $p>0.05$). The results are expressed as mean $\pm$ SD.

A comparison of the D^{2D} and D^{3D} values between the healthy and the osteoporotic populations was performed by

the Student's t-test distribution for independent samples with Levene's test for the equality of variances. The limit of significance was set at $p<0.05$.

In order to evaluate the age influence of the results for D^{2D} and D^{3D} between the healthy and the osteoporotic groups, the effect of including age as a covariable in a linear general model analysis was also tested. The relationship between the results of 2D and 3D fractal dimension parameters, radius BV/TV, and the spinal BMD for the osteoporotic patients was analyzed by a linear regression with the Pearson's product-moment correlation coefficient.

III. RESULTS

All MR acquisitions were valid for the calculation of D^{2D} and D^{3D} parameters. Significant differences were found for the D^{3D} parameter between the healthy and the osteoporotic populations ($p<0.001$) with higher values in the healthy group than in the osteoporotic group (2.33 ± 0.04 vs 2.27 ± 0.03, healthy vs osteoporotic; mean $\pm$ std). Although with less statistical significance, a clear dissimilarity was observed between the healthy and osteoporotic patients ($p=0.04$) for the D^{2D} parameter, with also higher values in the healthy group than in the osteoporotic population (1.55 ± 0.03 vs 1.50 ± 0.06, healthy vs osteoporotic; mean $\pm$ std). However, variances showed a trend to dissimilarity in this case ($p=0.08$). A representation of the result distribution for D^{2D} and D^{3D} in the healthy and osteoporotic groups can be observed in Fig. 4.

The differences for the D^{2D} and D^{3D} parameters were analyzed also with age influence correction on the results. No significant relationships were found between D^{2D}, D^{3D}, and age ($r=-0.02$, $p=0.94$ and $r=-0.31$, $p=0.18$; D^{2D} vs age, D^{3D} vs age). Significant differences were found between the healthy group and the patients with osteoporosis after correction for age is applied to the D^{3D} parameter ($p<0.001$). Also, a clear separation was obtained for the D^{2D} parameter with an increased significance ($p=0.02$) in comparison to the results obtained without age correction.

The BV/TV values obtained were higher in the healthy population than those obtained in the group of osteoporotic patients ($21.9\pm1.9\%$ vs $21.1\pm1.3\%$, healthy vs osteoporotic); however, there were no significant differences between groups ($p=0.29$).

A significant relationship was found between distal radius BV/TV parameter and spinal BMD (regression analysis; $r=0.64$, $p=0.02$). No significant association was observed between D^{2D}, D^{3D}, and BV/TV results (regression analysis; $r=0.34$, $p=0.13$ and $r=0.30$, $p=0.19$; D^{2D} vs BV/TV, D^{3D} vs BV/TV). In patients with osteoporosis, the relationship between fractal dimensions and BMD showed that the D^{2D} parameter was not significantly related to the spinal BMD measurements (regression analysis; $r=0.43$, $p=0.16$). However, a modest trend to a relationship was appreciated. The D^{3D} results also showed no association with the spinal BMD measurements (regression analysis; $r=0.23$, $p=0.48$), with a lower significance than D^{2D}.

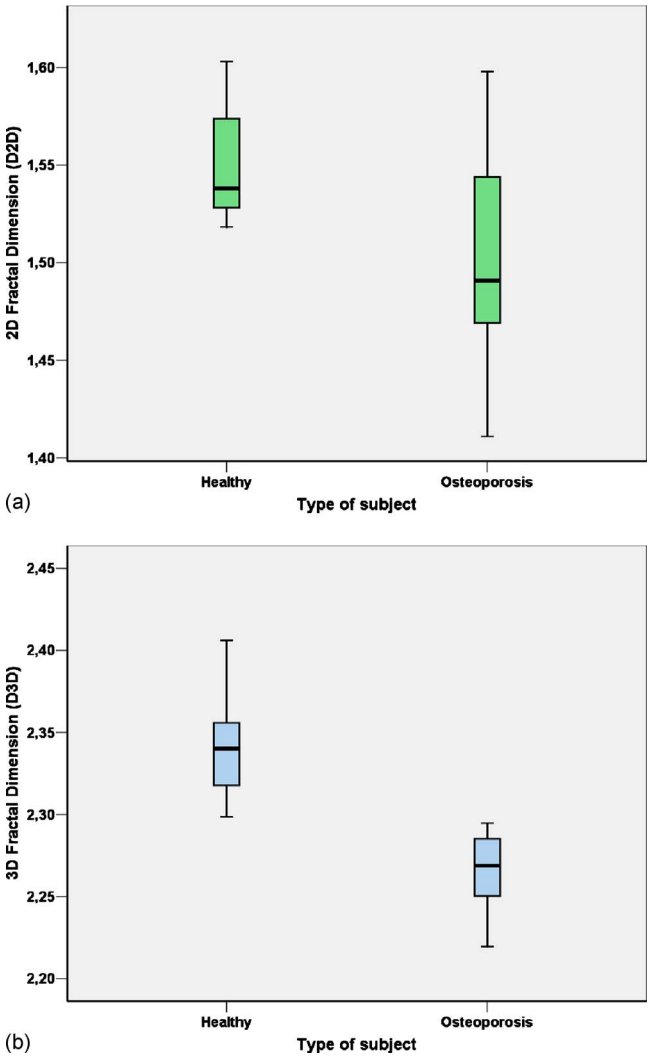

FIG. 4. Box-whisker plots showing the differences between the healthy and osteoporotic populations for the D^{2D} (a) and D^{3D} (b) parameters. Different dispersion data exist for the D^{2D} parameter between both groups.

IV. DISCUSSION

In this study, we have assessed the feasibility of 2D and 3D fractal analysis methods for the *in vivo* characterization of the trabecular bone structural complexity. Image processing techniques and box-counting algorithms have been implemented in order to quantify the D^{2D} and D^{3D} parameters of the cancellous bone from high-spatial resolution 3 T MRI acquisitions of the distal radius metaphysis. The D^{2D} and D^{3D} parameters have been found to significantly differentiate between healthy and osteoporotic conditions; furthermore, D^{3D} has shown better discrimination ($p<0.001$) between the healthy volunteers and the osteoporotic patients than D^{2D} ($p=0.04$). The D^{2D} and D^{3D} measurements were compared to radius BV/TV and spinal BMD results in the osteoporotic patients and no significant relationships were found, showing that D^{2D} and D^{3D} results probably provide a different kind of information complementary to the spinal BMD obtained with the current DXA examinations.

The calculation of D^{3D} values from high-spatial resolution

MRI measurements of trabecular bone was found to be feasible if applied after proper image processing and efficient contour detection algorithms. A low processing time was achieved easing the integration of the method in an automated trabecular bone fractal characterization processing sequence. To our knowledge, the application of 3D fractal measurements to the study of trabecular bone from MR acquisitions has not been previously investigated.

The values obtained for the D^{3D} parameter were significantly different between the healthy and osteoporotic groups ($p<0.001$), with lower values in the osteoporotic population (Fig. 4). In this sense, Ito *et al.*[4] obtained significant differences for the MDCT-derived D^{3D} parameter between women with and without history of osteoporotic fractures ($p<0.001$). Although with less significance, the D^{2D} results showed a clear statistical differentiation between both groups ($p=0.04$) (Fig. 4). This finding is comparable to the obtained by Majumdar *et al.*[19] where the D^{2D} parameter was found to be slightly different between healthy and osteoporotic postmenopausal populations ($p=0.01$) with lower values in the women with osteoporosis (1.43 ± 0.11 vs 1.55 ± 0.03, healthy; 1.34 ± 0.17 vs 1.50 ± 0.06, osteoporotic; Majumdar *et al.* vs our results, respectively). These significant differences were detected even with the large slice thickness of their acquisition, which was of 700 μm at a 1.5 T scanner. On the contrary, Hudelmaier *et al.*[25] did not observe significant differences between the results of the D^{2D} in a group of healthy volunteers compared to a group of patients with osteoporosis (1.72 ± 0.03 vs 1.71 ± 0.03, $p>0.05$; healthy vs osteoporotic, respectively). Their in-plane spatial resolution (156 μm) was exactly the same as that used by Majumdar *et al.*;[19] however, slice thickness was smaller (300 μm). Although in the calcaneus, Link *et al.*[26] found significant differences in the D^{2D} parameter between healthy and osteoporotic postmenopausal women ($p=0.007$) with lower values in the osteoporosis cases (1.66 ± 0.06 vs 1.61 ± 0.04; healthy vs osteoporotic, respectively). As several different definitions exist for the fractal dimension parameter, the used algorithm or method must always be carefully specified. Some authors found similar values with MR but several methodological differences exist between studies and an effective comparison of the results is not possible.[27] In this sense, in the works mentioned above[19,25,26] the box-counting algorithm was used for D^{2D} calculation, while the analysis of Pothuaud *et al.* was based on the fractional Brownian motion model and the evaluation of porosity was implemented by numerical dilation and removal processes to the 2D trabecular bone images.

The BV/TV from the distal radius trabecular bone showed a significant relationship with the spinal BMD, explaining a direct association between the bone density values at both locations. The BV/TV values showed no statistically significant differences between healthy and osteoporotic groups and were not significantly related to D^{2D} and D^{3D}. Despite the clear relationship between radius BV/TV and spinal BMD, the D^{2D} presented no significant relationship with the spinal BMD measurements performed in the patients group ($r=0.43$, $p=0.16$), although a modest trend to the association was observed. The D^{3D} also had no apparent relationship with the BMD measurements, with a lower association with BMD than D^{2D} ($r=0.23$, $p=0.48$), which could be preliminarily explained by the different structural information that might provide a 3D approach to the calculation of the fractal dimension compared to D^{2D} measurements. However, this conclusion should be considered as preliminary since the parameters have been measured at different locations. The work developed by Hudelmaier *et al.*[25] also found that the D^{2D} parameter was not related to BMD measurements (whereas other parameters like BV/TV or Tb.Th showed a relationship) and confirmed the independent information provided by D^{2D} if compared to BMD.

Our results suggest that for the fractal characterization of bone trabeculae complexity, a 3D approach should be used instead of the 2D box-counting algorithm. The data distribution variance in healthy and osteoporotic populations is more uniform for the 3D than in the 2D approach. In 2D, more dispersion is obtained in the patients group. The different variances observed in both parameters, with less data dispersion in the 3D approach, express that the D^{3D} is more accurate than the D^{2D} data for osteoporosis diagnosis.

The principal orientation of the trabecular bone in the radius corresponds to the longitudinal dimension.[28] If axial images are acquired with anisotropic spatial resolution, that is, with a slice thickness larger than the in-plane high-spatial resolution, the main orientation of the trabecular bone is being clearly underestimated. Even more, if a 2D approach is used for the fractal characterization, with the results averaged with all the slices, the main alignment direction of the trabeculae is also not taken into consideration. The combination of high-spatial isotropic resolutions in the acquisition of the images combined with a 3D postprocessing algorithm seems to be the most appropriate configuration for an efficient fractal characterization of the trabecular bone. Compared to 1.5 T, the high-spatial resolution images achievable with 3 T magnets in all three directions together with the increased SNR have allowed the implementation of D^{3D} quantification algorithms.

Some bias should be commented. First, the study cohort was small and only patients with osteoporosis but not osteopenia were included. Therefore, an analysis of the relationship between fractal dimensions and trabecular bone status of patients at initial stages of the disease could not be performed. A larger and better defined study cohort with different stages of the disease including additional data like the number of vertebral fractures would be relevant. This analysis would improve our knowledge about the behavior of the D^{2D} and D^{3D} parameters when cancellous bone structure starts to degenerate. Second, although age distributions of both groups analyzed (healthy vs osteoporotic) are not significantly different, a clear tendency to a difference existed, with higher ages in the group of osteoporotic patients. The influence of the age on the results was evaluated using a linear general model and significant differences were maintained between healthy and osteoporotic in the corrected sta-

tistical analysis of the fractal dimension parameters. A better age matching should be considered for the next studies in order to avoid possible confounding factors like age in the results. Also, BMD data were only obtained in the osteoporotic population and no DXA acquisitions were performed in the healthy subjects since they did not present previous history or symptoms of bone diseases. Although the analysis of the BMD differences between healthy and osteoporotic groups would put the BMD parameter into context and the comparison with the D^{2D} and D^{3D} parameters would be also interesting, our clinical workflow does not contemplate the use of ionizing radiations in a DXA scan without a clinical indication. Furthermore, the inclusion of male patients with trabecular bone deterioration abnormalities should also be useful for the characterization of abnormal bone resorption processes. We selected the wrist to obtain high resolution images because this region is close enough to the wrist-dedicated phased array coils. The acquisition of high-spatial resolution MR images in larger regions with more distance between the coil and the tissue of interest is limited by the noise, therefore adding difficulties to the image post processing and analysis. Finally, the fractal dimension parameters should be combined with other morphometric or mechanical variables in order to perform a direct approach to the evaluation of the fracture risk.

In conclusion, 2D and 3D implemented methods for the calculation of the fractal dimension parameter may be used for the fractal characterization of the trabecular bone network. Both D^{2D} and D^{3D} parameters were found to be influenced by the disease, with a better differentiation for the 3D method. Finally, the D^{3D} parameter has probably a different substrate regarding the trabecular bone status not explained by the BMD alone. These results may set the 3D approach combined with high resolution MRI as the recommended method for the *in vivo* fractal dimension characterization of the trabecular bone structure in patients with osteoporosis.

ACKNOWLEDGMENTS

The authors would like to thank the following financial support: Vicerectorat d'Innovació i Desenvolupament of the Universitat Politècnica de València (Contract No. PAID-06-07/3104), Grupos Emergentes—Generalitat Valenciana (Grant No. GV/2009/126), Instituto de la Mediana y Pequeña Industria Valenciana (IMPIVA) of the Generalitat Valenciana (Contract No. IMIDTP/2009/334), and Spanish Ministry of Science through Project No. TEC2009-14128.

[a]Author to whom correspondence should be addressed. Electronic mail: aalberich.val@quiron.es; Telephone: +34963390405; Fax: +34963391147.

[1]J. Y. Reginster and N. Burlet, "Osteoporosis: A still increasing prevalence," Bone **38**, 4–9 (2006).
[2]E. Seeman, "Invited Review: Pathogenesis of osteoporosis," J. Appl. Physiol. **95**, 2142–2151 (2003).
[3]F. W. Wehrli, "Structural and functional assessment of trabecular and cortical bone by micro magnetic resonance imaging," J. Magn. Reson Imaging **25**, 390–409 (2007).
[4]M. Ito, K. Ikeda, M. Nishiguchi, H. Shindo, M. Uetani, T. Hosoi, and H. Orimo, "Multi-detector row CT imaging of vertebral microstructure for evaluation of fracture risk," J. Bone Miner. Res. **20**, 1828–1836 (2005).
[5]S. Boutroy, M. L. Bouxsein, F. Munoz, and P. D. Delmas, "In vivo assessment of trabecular bone microarchitecture by high-resolution peripheral quantitative computed tomography," J. Clin. Endocrinol. Metab. **90**, 6508–6515 (2005).
[6]A. Alberich-Bayarri, L. Marti-Bonmati, R. Sanz-Requena, E. Belloch, and D. Moratal, "In vivo trabecular bone morphologic and mechanical relationship using high-resolution 3-T MRI," AJR, Am. J. Roentgenol. **191**, 721–726 (2008).
[7]A. Laib, D. C. Newitt, Y. Lu, and S. Majumdar, "New model-independent measures of trabecular bone structure applied to in vivo high resolution MR images," Osteoporosis Int. **13**, 130–136 (2002).
[8]G. J. Kazakia, B. Hyun, A. J. Burghardt, R. Krug, D. C. Newitt, A. E. de Papp, T. M. Link, and S. Majumdar, "In vivo determination of bone structure in postmenopausal women: A comparison of HR-pQCT and high-field MR imaging," J. Bone Miner. Res. **23**, 463–474 (2008).
[9]P. A. Hulme, S. K. Boyd, and S. J. Ferguson, "Regional variation in vertebral bone morphology and its contribution to vertebral fracture strength," Bone **41**, 946–957 (2007).
[10]B. R. Gomberg, P. K. Saha, H. K. Song, S. N. Hwang, and F. W. Wehrli, "Topological analysis of trabecular bone MR images," IEEE Trans. Med. Imaging **19**, 166–174 (2000).
[11]J. Carballido-Gamio, R. Krug, M. B. Huber, B. Hyun, F. Eckstein, S. Majumdar, and T. M. Link, "Geodesic topological analysis of trabecular bone microarchitecture from high-spatial resolution magnetic resonance images," Magn. Reson. Med. **61**, 448–456 (2009).
[12]P. K. Saha and F. W. Wehrli, "A robust method for measuring trabecular bone orientation anisotropy at in vivo resolution using tensor scale," Pattern Recogn. **37**, 1935–1944 (2004).
[13]S. Majumdar, R. S. Weinstein, and R. R. Prasad, "Application of fractal geometry techniques to the study of trabecular bone," Med. Phys. **20**, 1611–1619 (1993).
[14]D. C. Newitt, S. Majumdar, B. van Rietbergen, G. von Ingersleben, S. T. Harris, H. K. Genant, C. Chesnut, P. Garnero, and B. MacDonald, "In vivo assessment of architecture and micro-finite element analysis derived indices of mechanical properties of trabecular bone in the radius," Osteoporosis Int. **13**, 6–17 (2002).
[15]G. P. Feltrin, V. Macchi, C. Saccavini, E. Tosi, C. Dus, A. Fassina, A. Parenti, and R. De Caro, "Fractal analysis of lumbar vertebral cancellous bone architecture," Clin. Anat. **14**, 414–417 (2001).
[16]B. B. Mandelbrot, *The Fractal Geometry of Nature* (Freeman, New York, 1982).
[17]D. Chappard, E. Legrand, B. Haettich, G. Chalès, B. Auvinet, J. P. Eschard, J. P. Hamelin, M. F. Baslé, and M. Audran, "Fractal dimension of trabecular bone: Comparison of three histomorphometric computed techniques for measuring the architectural two-dimensional complexity," J. Pathol. **195**, 515–521 (2001).
[18]S. Majumdar, J. Lin, T. Link, J. Millard, P. Augat, X. Ouyang, D. Newitt, R. Gould, M. Kothari, and H. Genant, "Fractal analysis of radiographs: Assessment of trabecular bone structure and prediction of elastic modulus and strength," Med. Phys. **26**, 1330–1340 (1999).
[19]S. Majumdar, H. K. Genant, S. Grampp, D. C. Newitt, V. H. Truong, J. C. Lin, and A. Mathur, "Correlation of trabecular bone structure with age, bone mineral density, and osteoporotic status: In vivo studies in the distal radius using high resolution magnetic resonance imaging," J. Bone Miner. Res. **12**, 111–118 (1997).
[20]H. Follet, K. Bruyère-Garnier, F. Peyrin, J. P. Roux, M. E. Arlot, B. Burt-Pichat, C. Rumelhart, and P. J. Meunier, "Relationship between compressive properties of human os calcis cancellous bone and microarchitecture assessed from 2D and 3D synchrotron microtomography," Bone **36**, 340–351 (2005).
[21]S. Banerjee, S. Choudhury, E. T. Han, A. C. Brau, C. V. Morze, D. B. Vigneron, and S. Majumdar, "Autocalibrating parallel imaging of in vivo trabecular bone microarchitecture at 3 Tesla," Magn. Reson. Med. **56**, 1075–1084 (2006).
[22]B. Vasilic and F. W. Wehrli, "A novel local thresholding algorithm for trabecular bone volume fraction mapping in the limited spatial resolution regime of in-vivo MRI," IEEE Trans. Med. Imaging **24**, 1574–1585 (2005).
[23]S. N. Hwang and F. W. Wehrli, "Subvoxel processing: A method for reducing partial volume blurring with application to in vivo MR images of trabecular bone," Magn. Reson. Med. **47**, 948–957 (2002).
[24]N. Otsu, "A threshold selection method from gray-level histogram," IEEE Trans. Syst. Man Cybern. **9**, 82–86 (1979).

[25]M. Hudelmaier, A. Kollstedt, E. M. Lochmüller, V. Kuhn, F. Eckstein, and T. M. Link, "Gender differences in trabecular bone architecture of the distal radius assessed with magnetic resonance imaging and implications for mechanical competence," Osteoporosis Int. **16**, 1124–1133 (2005).
[26]T. M. Link, S. Majumdar, P. Augat, J. C. Lin, D. Newitt, Y. Lu, N. E. Lane, and H. K. Genant, "In vivo high resolution MRI of the calcaneus: Differences in trabecular structure in osteoporosis patients," J. Bone Miner. Res. **13**, 1175–1182 (1998).
[27]L. Pothuaud, C. L. Benhamou, P. Porion, E. Lespessailles, R. Harba, and P. Levitz, "Fractal dimension of trabecular bone projection texture is related to three-dimensional microarchitecture," J. Bone Miner. Res. **15**, 691–699 (2000).
[28]W. G. Geraets, P. F. Van der Stelt, P. Lips, P. J. Elders, F. C. Van Ginkel, and E. H. Burger, "Orientation of the trabecular pattern of the distal radius around the menopause," J. Biomech. **30**, 363–370 (1997).